Journal of Building Performance Simulation
Vol. xx, No. xx, xx xx, 1–27

Article

Rule-based demand side management of domestic hot water production with heat pumps in zero energy neighbourhoods

R. De Coninck[a,b*], R. Baetens[c], D. Saelens[c], A. Woyte[b] and L. Helsen[a]

[a]*Applied Mechanics and Energy Conversion, Department of Mechanical Engineering, KU Leuven, Belgium*; [b]*3E, Brussels, Belgium*; [c]*Building Physics Section, Department of Civil Engineering, KU Leuven, Belgium*;

(*Accepted version of May 3, 2013*)

Grid saturation has been reported in electricity distribution systems with a high penetration of photovoltaic (PV) systems. This saturation is often caused by overvoltage and results in curtailing or shutting-down of the PV inverters, leading to a loss of renewable electricity generation.

The presented work assesses the potential of rule-based demand side management (DSM) applied to domestic hot water (DHW) production with heat pumps in dwellings for reducing the non-renewable energy use of the neighbourhood.

The studied case consists of 33 single-family dwellings connected to the IEEE 34 node test feeder in a moderate European climate. Each dwelling is designed as a net zero energy building (NZEB) by adequate design of a heat pump and PV system.

A detailed dynamic simulation model is implemented by use of a cross domain Modelica library for integrated district energy assessment. The user behaviour is obtained from a stochastic model based on Markov chains and survival analysis. Different rule-based DSM control strategies are applied to the individual dwelling's DHW systems.

The results show that for balancing the PV production, active thermal energy storage in the DHW storage tanks is very promising. Even with very basic control algorithms and small storage tanks of 0.3 m^3, curtailing losses can be reduced by 74 %. This represents a net energy saving on neighbourhood level of 3.4 %.

Keywords: demand side management (DSM), rule-based control, photovoltaics (PV), Modelica, thermal energy storage (TES), integrated neighbourhood simulation

Acknowledgment (AAM)

This is an Author's Accepted Manuscript (AAM) of an article accepted for publication by the Journal of Building Performance Simulation [copyright Taylor & Francis]. This article includes modifications as a result of the peer review process organised by the publisher. The Journal of Building Performance Simulation is available online at `http://www.tandfonline.com/loi/tbps20`.

1. Introduction

1.1 Grid saturation due to overvoltage

Distributed electricity generation (DG) affects the operating conditions of distribution grids in different ways (Dugan and McDermott, 2001; Ackermann and Knyazkin, 2002). One specific

*Corresponding author. Email: roel.deconinck@mech.kuleuven.be

ISSN: 1940-1493 print/ISSN 1940-1507 online
© xx Taylor & Francis
DOI: 10.1080/1940149YYxxxxxxxx
http://www.informaworld.com

issue consists of steady-state voltage rises, which are of particular interest in distribution grids with a large amount of PV systems (Woyte et al., 2006; Caamaño Martin et al., 2008). At times of high solar radiation, these voltage rises may result in a shut down of some of the PV inverters, or a curtailing of the output power by droop control (De Brabandere et al., 2004). These problems will happen more frequently as the cumulative installed PV capacity is expected to keep on rising in existing distribution grids (EPIA, 2012).

As a result of the European policy regarding building energy performance, low energy neighbourhoods will have to become the standard for new construction from 2020 onwards (European Parliament, 2010). In these low energy buildings and neighbourhoods, PV and heat pump technology are often combined in order to reach a yearly 'net zero' energy balance. However, this may lead to inverter shut down or droop control at certain times, causing a loss of renewable electricity generation. For example, Baetens et al. (2012) computed a loss of 14 % to 47 % of the expected local PV electricity generation in a low energy neighbourhood, depending on feeder sizing and parameter settings for the overvoltage shut-down.

Possible solutions to reduce the amount of curtailed power in distribution grids with a large amount of PV systems consist of:

- Feeder reinforcements
- Changing the transformer tap positions to obtain an adapted voltage at the point of common coupling
- Active voltage control with modern inverters (Bletterie et al., 2010)
- Demand side management (DSM)

This paper assesses the potential of rule based DSM applied to the domestic hot water (DHW) production in dwellings with heat pumps. The aim of load shifting is not the voltage control on itself, but a reduction of the non-renewable energy use of the neighbourhood.

1.2 Demand side management

The idea of DSM for this case is straightforward: by shifting electrical loads to time periods of excessive voltage in the grid, curtailing of the inverters can be avoided. There are different options for the shiftable loads. This paper will neither consider load shifting with household appliances like dishwashers, cloth washers and dryers, nor by use of an electrical battery.

The shiftable load is the compression heat pump that produces heat for space heating and DHW. This paper only considers the DHW production as a shiftable load. The required flexibility to enable the decoupling of heat generation and consumption is the thermal energy storage (TES) tank for storage of the domestic hot water. We only consider DHW and exclude space heating from this paper because the latter requires a more detailed analysis in order to cover the different emission systems and control strategies which lies beyond the scope of this paper. As will be shown, the potential of load shifting on DHW is substantial and justifies the current scope. The application of the elaborated methodology on space heating is a topic for future work.

In a previous study, different control strategies had been applied to a heat pump for space heating in a single dwelling (De Coninck et al., 2010). Although it was shown that peak loads can be reduced at the level of an individual building, the impact of these control strategies on the distribution grid and consequently the inverter behaviour could not be assessed. This paper takes the next step by modelling the entire neighbourhood.

1.3 Modelling of neighbourhoods

Simulations or optimizations on a single building level cannot be used to study the operation of the distribution grid. DSM studies on single buildings can be used to study the energy or cost savings in that building, up to the power exchange with the grid. It is however incorrect to use these studies for drawing conclusions about the ability of DSM to compensate for stochastic

electricity generation or distribution grid loads. For this purpose, a neighbourhood model is required, composed of the distribution grid, different buildings and stochastic user behaviour.

On the other hand, neighbourhood (or district) level simulations are not new. Manfren et al. (2011) discuss different aspects of district level simulations whereas Baetens et al. (2012) give a good overview of existing approaches and tools.

DSM applied to heat pumps has to be studied with detailed dynamic models. These models need to include the building, heating, ventilation and air-conditioning (HVAC) and user behaviour. This is required for capturing the interaction between the heating system and the building, the effects of ambient, inside and TES tank temperatures on the heat pump efficiency, the consequences of on/off cycling, etc. Most district simulation tools cannot cope with the desired level of detail in the building model. On the other hand, typical building simulation tools do not allow to model multiple buildings connected to a distribution grid. In order to combine the best of two worlds, we use Modelica.

The present paper shows how thermal energy management can be applied in order to relieve grid saturation on neighbourhood level. Special attention is paid to the modelling of the DHW system because both the hot water demand and the TES tank model largely influence the potential of DSM. Modelica has proven well suited for this purpose.

2. Model

2.1 Overview

The model consists of 33 single-family dwellings connected to the 34-node test feeder of the Institue of Electrical and Electronics Engineers (IEEE) (Kersting, 2001) in the moderate European climate of Uccle, Belgium. It is assumed that all dwellings are identical, built according to a low-energy standard, heated with a modulating air-to-water heat pump and equipped with a PV system covering their complete yearly energy needs. The following paragraphs elaborate on the modelling principles and details, whereas Tables 1 and 2 give an overview of the building and general model parameters respectively.

2.2 Dwelling

A single dwelling typology is used which was identified in the European TABULA project (Loga et al., 2009) as representative for semi-detached single-family houses constructed after the year 2005. This means that all dwellings are identical and that the variation in temperature and load is caused entirely by the stochastic user behaviour. The dwelling has a total heated floor area of $196\,\mathrm{m}^2$, a total volume of $643\,\mathrm{m}^3$, a compactness of $1.58\,\mathrm{m}$ and is modelled as a single thermal zone. The dwelling is designed according to a low-energy standard and has massive walls and floors. The composition of the different envelope elements and resulting U-values are given in Table 1.

We suppose an air-tightness corresponding to the low energy standard with a natural infiltration rate of 0.03 air changes per hour (ACH). All dwellings are equipped with mechanically balanced, air-to-air heat-recovery ventilation with an air change rate of 0.5 ACH and a recovery efficiency of 0.84.

All dwellings have exterior solar screens with a solar transmittance of 0.24. As a result no active cooling needs to be installed in the dwellings. The automated exterior solar screen is lowered at a global horizontal irradiation level of $250\,\mathrm{W/m}^2$ and raised again at an irradiation level below $150\,\mathrm{W/m}^2$.

Table 1. Overview of building model parameters

Element	A (m^2)	U ($W/(m^2\,K)$)	g (-)
Outer facade [a]	135.0	0.22	-
Floor [b]	98.0	0.19	-
Roof [c]	118.0	0.11	-
Windows	33.5	1.10	0.59

[a] 15 cm of PUR between an 8 cm outer and 14 cm inner brick wall.

[b] 10 cm of PUR below a 8 cm screed layer and on a 20 cm concrete slab.

[c] 30 cm of mineral wool between multiplex plates in a timber frame construction.

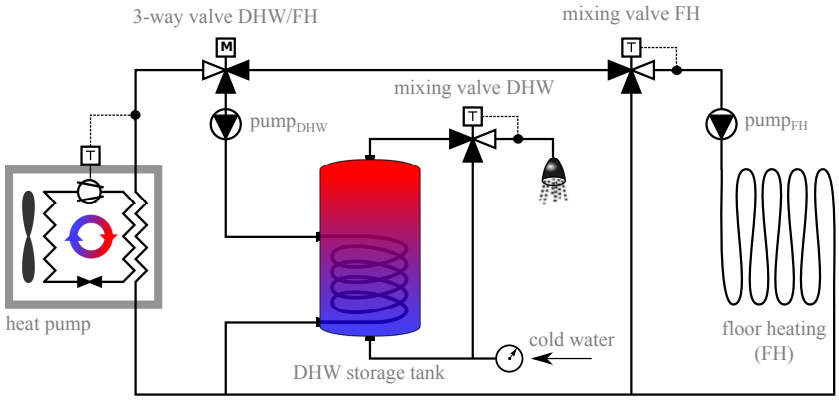


Figure 1. Hydraulic scheme of the heating and DHW system

2.3 HVAC system

Each of the 33 dwellings has an identical space heating and DHW system, visualized in Figure 1. Heat is produced by means of a modulating air-to-water heat pump (HP), connected to a floor heating and a DHW storage tank.

2.3.1 Heating

The heat pump model is based on linear interpolation in a performance map retrieved from manufacturer data (Daikin Europe N.V., 2006). The performance map does not take into account (de)frosting of the evaporator as shown in Figure 2 (although it does extend to negative ambient temperatures). The nominal coefficient of performance (COP) is 3.17 at 2/35 °C and 2.44 at 2/45 °C test conditions (i.e. air/water temperature) for full load operation. The thermal power of the heat pump is 3459 W at 2/35 °C.

The interpolation in the performance map defines the heating power $\dot{Q}_{net}$ (W) and electricity use $\dot{P}_{net}$ (W) as a function of condenser outlet temperature, the ambient temperature and modulation level (between 25 % and 100 %). The heat pump can modulate thanks to an inverter at the compressor. In the model, the modulation level mod_{final} (%) is obtained in two steps. First, the initial modulation mod_{init} (%) is computed according to Equation (1), and then limited according to Equation (2). To avoid on/off cycling, a hysteresis is added to the starting condition: the heat pump will only start when $mod_{init} \geq 50\%$.

$$mod_{init} = \frac{\dot{Q}_{demand}}{\dot{Q}_{max}} = \frac{\dot{m} c_p (T_{set} - T_i)}{f(T_{evap}, T_c)} \tag{1}$$

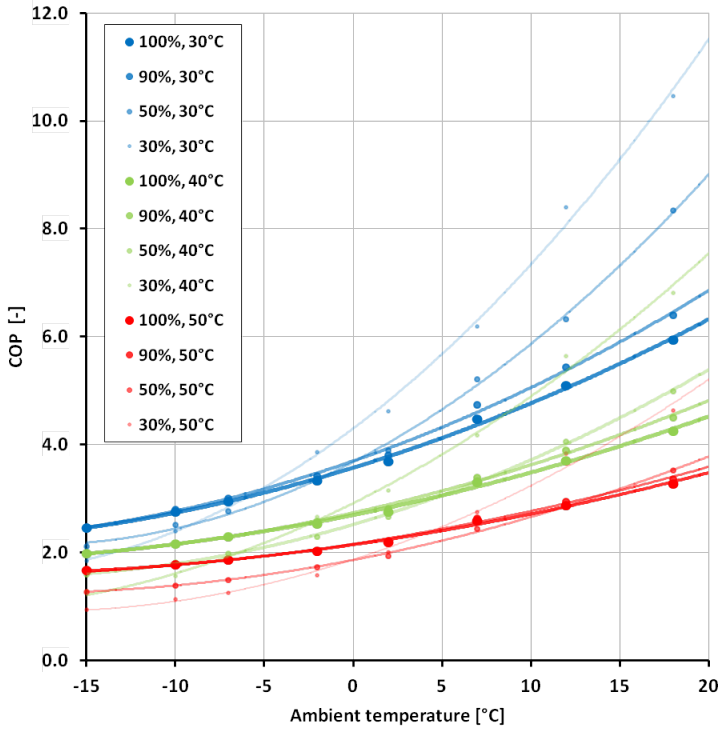


Figure 2. Performance map of the heat pump, showing the COP as a function of ambient temperature for different modulation levels (30 %, 50 %, 90 % and 100 %) and different condenser outlet temperatures (30 °C, 40 °C and 50 °C).

$$mod_{final} = \begin{cases} 0\%(=\text{off}) & \text{if } mod_{init} < 25\%, \\ 100\% & \text{if } mod_{init} \geq 100\%, \\ mod_{init} & \text{else.} \end{cases} \tag{2}$$

In these equations, $\dot{m}$ (kg/s) is the mass flow rate in the condenser, c_p (J/(kg s)) the specific heat capacity of water, T_{set} (K) is the condenser set temperature, T_i (K) is the condenser inlet temperature, $\dot{Q}_{demand}$ (W) is the demanded thermal power and $\dot{Q}_{max}$ (W) is the maximum thermal power at the current evaporator temperature T_{evap} (K) and condenser temperature T_c (K), obtained from the performance map.

The model takes into account the water content of the condenser m_c (kg) and dry capacity c_{dry} (J/K), both connected to the environmental temperature T_e (K) through a thermal conductance UA_{loss} (W/K) in order to obtain a dynamic model with heat losses according to Equation (3).

$$(m_c c_p + c_{dry})\frac{dT_c}{dt} = \dot{m} c_p (T_i - T_c) + \dot{Q} - UA_{loss}(T_c - T_e) \tag{3}$$

In this equation, $\dot{Q}$ (W) is the condensation heat $\dot{Q}_{net}$ augmented with the environmental heat losses $UA_{loss}(T_c - T_e)$. This ensures that the steady state efficiency of the heat pump is identical to the performance data, while adding environmental losses and dynamics to the model. The produced heat is used for charging the floor heating, designed to work at a 35/30 °C regime at design conditions and for charging the domestic hot water storage tank. As mentioned above, the investigated DSM controls only concern the charging of the DHW tank.

2.3.2 Domestic hot water and storage tank

The stratified water energy storage tank is only used for DHW production. It is connected to the heat pump through an internal heat exchanger, and the hot water is withdrawn via a thermostatic mixing valve in order to obtain water at 45 °C. A one-dimensional multinode storage tank model is used. For each node i (numbering starts at the top), the energy balance and mass balance equations are given in respectively Equations (4) and (5) and presented schematically in Figure 3.

$$m_i c_p \frac{dT_i}{dt} = \sum_j c_p \dot{m}_j T_j + \dot{Q}_{cond,i-1} + \dot{Q}_{cond,i} + \dot{Q}_{buo,i} + \dot{Q}_{buo,i-1} + \dot{Q}_{env,i} + \dot{Q}_{HX,i} \quad (4)$$

$$\sum_j \dot{m}_j = 0 \quad (5)$$

In these equations, m_i (kg) is the water mass of the node i with temperature T_i (K) and c_p is the specific heat of water, assumed to be constant and equal to $4177\,\mathrm{J\,kg^{-1}\,K^{-1}}$. The in- and outgoing water flows in node i due to forced circulation are represented by $\dot{m}_j$ (kg/s), their corresponding temperatures by T_j (K) (for outgoing flows, $T_j = T_i$). Heat transfer to neighbouring nodes via conduction is given by $\dot{Q}_{cond}$ (W). Transmission losses to the environment are given by $\dot{Q}_{env,i}$ (W). When the node i contains a section of the internal heat exchanger, the heat transfer from this section into the node is given by $\dot{Q}_{HX,i}$ (W). $\dot{Q}_{buo}$ (W) is the equivalent heat transfer to neighbouring nodes due to buoyancy effects and this term will be elaborated in the following paragraphs. Mass flow rates and heat fluxes entering the node i have a positive sign.

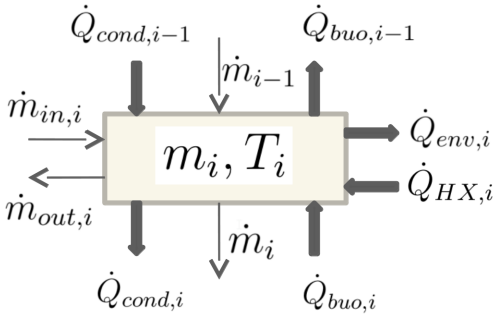


Figure 3. Schematic overview of the nodal energy balance in the TES tank

The storage tank plays a key role in the DSM strategies, therefore specific attention was paid to verification and calibration of the model to manufacturer data. The goal of this calibration is to obtain a robust model formulation, that can be used for different storage volumes. This requires that the model parameters are independent of the size and geometry of the nodes.

Technical information and measurements from the commercial DHW tank Vitocell 100-V, type CVW of 390 l are used to tune the parameters of the model (Viessmann, 2011).

Firstly, geometrical details like tank diameter and height, surface and water content of the internal heat exchanger are set. The heat transfer coefficients of the internal heat exchanger (internal convection, conduction and external convection) are calculated based on heat transfer correlations.

Secondly, the parameters for the transmission losses $\dot{Q}_{\mathrm{env},i}$ are set. In order to obtain a parametric model that allows scaling, a fixed $UA_{fix}(\mathrm{W\,K^{-1}})$ and a surface dependent heat loss coefficient $U_{Ins}(\mathrm{W\,m^{-2}\,K^{-1}})$ are defined. U_{Ins} depends on thickness and thermal conductivity

of the insulation. UA_{fix} accounts for cold bridges and increased heat losses at the connections and is fixed to match the given 24 hour heat losses according to DIN V 18599.

Finally, the remaining parameters to be set are the number of layers and the buoyancy model, which are linked. The aim of this calibration exercise is to find a model with a relatively low number of layers that is robust to changes in storage volume. Therefore, the number of layers and the buoyancy formulation should not influence the yearly performance of the storage tank (or only to a limited extend). Thermal stratification and buoyancy are complex processes depending on tank geometry and operation conditions. Haller et al. (2009) review different methods that have been proposed to characterize thermal stratification in TES tanks. All attempts to include these phenomena in one-dimensional stratified storage tank models are strong simplifications of the 3-D flow patterns that occur (Han et al., 2009). Most one-dimensional stratified storage tank models approximate buoyancy effects as mixing between the layers in case of temperature inversion (Zurigat et al., 1989). In case of a fixed time step simulation, the mixing rate depends on the node volume and simulation time step (Newton, 1995; Mather et al., 2002). In case of continuous time solvers, a parameter is required for the time constant of mixing (Wetter, 2009). Specific buoyancy formulations exist for modelling plume entrainment, caused by the inflow of cold water at the top of the tank (Kleinbach et al., 1993). Kleinbach et al. (1993) and Mather et al. (2002) demonstrate the importance of the number of nodes with regard to accuracy of the model and more specifically the rate of stratification. This stratification plays an important role in the efficiency of the tank and as a consequence the total system (Rosen et al., 2004).

The technical sheet specifies four performance characteristics to tune the model: two discharging and two charging experiments. The discharging experiments show that the number of layers should be as high as 20 or even 40 in order to correctly model the sharp thermocline in discharging situations. However, we will show later that with the correct buoyancy model, a lower number of layers (down to 10 layers) does not have a significant impact on the yearly energy use and DHW comfort. The DHW comfort is defined as the ratio of DHW use at temperatures of at least 40 °C to the total DHW use.

As we model a tank with internal heat exchanger, the buoyancy model can be validated from the two charging experiments (a and b). In a first step, a buoyancy model is chosen, with unknown parameters. For each number of layers, a numeric optimization is carried out to find the optimal model parameters that minimize the sum of the residuals for both experiments a and b. The residual is the difference between the simulated and the specified tank outlet temperature at the final charging time.

We want to find a stable buoyancy formulation, meaning that the model parameters are independent of the number of nodes (between 5 and 40). However, for most buoyancy models, including time constant based node mixing, this is not the case and parameter variations of more than 100 % occur when the number of nodes is divided by two. A buoyancy model that leads to a parameter variability of less than 20 % is presented by Equation 6.

$$Q_{buo,i} = k_{buo}(N)\Delta T_i N^{1.5} \tag{6}$$

In this equation $Q_{buo,i}$ is the heat flow from layer $i+1$ to layer i, ($i = 1$ is top layer), $k_{buo}(N)$ is the model parameter to be identified which depends on N, the number of layers in the model and ΔT_i is the temperature difference between layer $i+1$ and layer i, i.e. zero if no temperature inversion. The resulting optimized $k_{buo}(N)$ as a function of N is shown in Figure 4. Two conclusions can be drawn from this figure: (i) for each number of layers between 5 and 40, a $k_{buo}(N)$ can be found for which the model closely matches the measurements, and (ii) the identified $k_{buo}(N)$ lie all in the interval of $20.8 \pm 20\,\%$.

With the optimal $k_{buo}(N)$ the impact of the number of nodes on the yearly performance of the tank can be analysed. Three different DHW tap profiles are defined (see 2.5.3). Figure 5 shows that for each of these profiles, reducing the number of layers from 40 to 10 will result

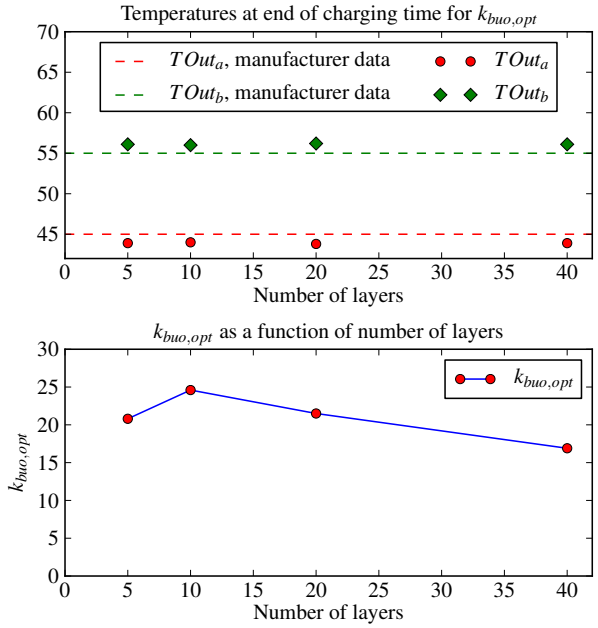


Figure 4. Top: model deviation from the validation data as a function of number of layers. Bottom: optimal $k_{buo}(N)$ according to Equation 6 as a function of number of layers.

in deviations on yearly energy use and DHW discomfort of less than 5 % and 2 % respectively. This is an important result, because neighbourhood simulations with 40 layers in each TES tank require significantly longer computation times.

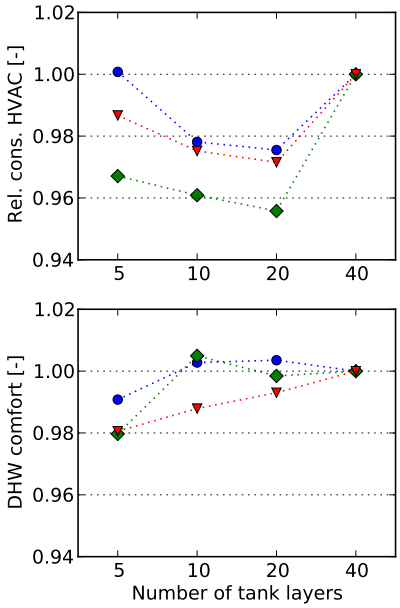


Figure 5. Sensitivity of the yearly energy use and DHW comfort to the number of layers if the optimal $k_{buo}(N)$ is taken according to Figure 4.

Finally, the robustness of the buoyancy model with parameter $k_{buo}(N)$ is checked around $k_{buo,10}$. For each of the three DHW profiles used in Figure 5 and for a constant tank volume,

the tank height and the number of layers is varied to check the sensitivity of $k_{buo,10}$ for small deviations in layer size and height. The results, given in Figure 6, show that small variations in geometry and discretization lead to deviations on yearly energy use and DHW discomfort of less than 2 % and 1 % respectively. These results confirm the robustness of the buoyancy formulation and the stratified storage tank model in general. No additional model enhancements to avoid numerical dissipation have been implemented.

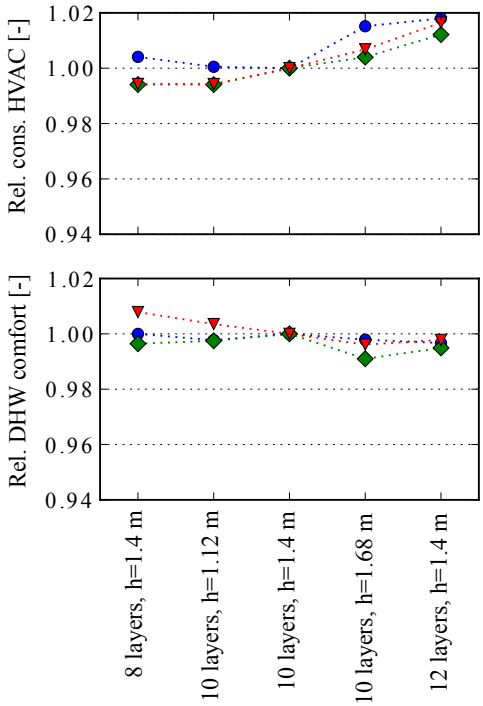


Figure 6. Sensitivity of the yearly energy use and DHW comfort to number of layers and TES tank height for $k_{buo,10}$

This parameter calibration was only done for a 390 l tank and corresponding internal heat exchanger. In this study, it is assumed that the heat exchanger and insulation thickness remain the same for changes in tank volume between 300 l and 500 l. All resulting parameters are found in Table 2 (on page 13).

2.3.3 Control

There are two loops in the HVAC control. The first loop controls the flow rate through the heat pump by sending on/off control signals to $pump_{FH}$ and $pump_{DHW}$. The signal for $pump_{FH}$ is sent by the room thermostat based on the operative temperature, set point and a hysteresis of 1 K (above set point). All dwellings have a constant temperature set point of 20 °C. This approach is chosen for reasons of simplicity given the fully stochastic user presence in combination with floor heating. Moreover, night set back is difficult to implement and has a limited impact in heavy-construction well-insulated and air-tight buildings (Olesen, 2001; Hastings, 2004). The signal for $pump_{DHW}$ is based on the measured and set point values for the storage tank top temperature T_{Top}, measured in the second layer. A hysteresis of 2 K is applied (above set point).

The second loop controls the condenser set temperature. This control is only active when the heat pump condenser receives a flow rate, and distinction is made based on which pump is running. When $pump_{FH}$ is activated, the set point follows a heating curve for space heating, but with an offset of 2 K in order to compensate for distribution losses. When $pump_{DHW}$ is activated, the set point is 5 K higher than the DHW tank set point in order to be able to reach the switch off condition on T_{Top}. Both pumps can be activated simultaneously. When this

happens, the condensor of the heat pump receives the sum of both flow rates and the highest temperature set point precedes.

For the reference case, the DHW tank set point $TSet_{DHW}$ results from a small sensitivity study. The tank set point has a large impact on the operation of the heat pump. If $TSet_{DHW}$ is low, the COP will be higher, but the heat pump will cycle more since after each DHW draw, the tank top temperature will be below the set point. This cycling behaviour will decrease the overall seasonal performance factor (SPF). A low set point will also decrease the DHW comfort (see Section 3.1). A few simulations with different DHW tap profiles led to the conclusion that for the reference case, a fixed DHW tank set point of 53 °C gives a satisfactory trade-off between thermal comfort and energy use.

2.4 Electricity generation

Each dwelling has a building integrated PV system which is sized to cover, on a yearly basis, the total electricity consumption of the dwelling. As the user behaviour influences this consumption, each dwelling will have a different installed PV capacity. Azimuth and inclination of the modules are identical for all dwellings.

The PV system is modelled with the 5-parameter model of De Soto et al. (2006) based on a temperature-dependent diode equivalent circuit (Sera et al., 2007). The efficiency parameters of a PV module are taken from manufacturer characteristics (Sanyo, 2008). The direct current power output of the modules is converted to AC power by means of an inverter with constant efficiency of 95 %.

To avoid excessive feeder voltages, the inverter is switched off when the voltage at the dwelling-feeder interface reaches a predefined limit. This switching-off is applied as the distribution system operator currently does not allow the distributed sources to provide voltage control of the distribution feeder, e.g. by reactive power control. This limit is set at an increase of 10 % of the nominal feeder voltage or 253 V according to national regulations on AREI Art.§235, the Belgian General Regulations for Electrical Installations (and Labour Protection). The inverter control is given a minimal off-time of roughly 300 s before trying to switch on again. To obtain a stable model, each of the 33 inverters has a slightly different off-time between 275 s and 318 s.

2.5 Occupant behaviour

The stochastic behaviour of accommodated occupants concerning presence, the use of appliances and lighting, and domestic hot water withdrawal is implemented as a combination of survival analyses for occupancy and embedded discrete-time Markov chains for the remainder.

2.5.1 Presence

Differently from earlier work (Baetens et al., 2012), occupancy is no longer described based on discrete-time Markov chains. The required differentiation based on household typologies results in a more comprehensive representation of occupancy behaviour at household level and a more realistic representation of the simultaneity of the resulting power demand for space heating and DHW.

Four different family types have been defined based on the work of Cheng and Steemers (2011), ie. (1) a young couple both working full time during weekdays and partly present in the weekend, (2) a family of 4 persons of which one parent works part time, (3) an unemployed couple and (4) a retired couple. For each family type, the average number of persons at home are defined for a typical weekday and a typical weekend. In order to obtain fully stochastic profiles, an uncertainty is applied to the average arrival and departure times for each household and an uncertainty to the average arrival and departure times for each day of the week for the survival analysis. Both uncertainties are defined by a standard deviation σ of 1 hour compared to the family type average and household average respectively. This results in all different occupancy

profiles, while the aggregated profiles by family type still reflect the typical days. To illustrate the result, a weekly aggregated occupancy profile for a single family of type (1) is given in Figure 7 and for a single family of type (4) in Figure 8.

2.5.2 Household electricity load

The implemented stochastics are consistent with Richardson et al. (2010) and are based on discrete-time Markov chains as described by Baetens et al. (2012). The resulting outputs are activity of the building occupants, the use of appliances (Richardson et al., 2010) and the use of lighting (Stokes et al., 2004; Richardson et al., 2009), and (only) depend on the household size, the present appliances and fixtures, whether it is a weekday or weekend day and global irradiances. Here, the use of appliances and lighting has a 1 minute resolution. To generate 33 statistically relevant profiles, bottom-up data concerning household size and installed appliances are used based on Belgian (FOD Economie, 2008) and European (Richardson et al., 2010) statistics on household sizes and appliance ownership rates respectively. As such, the main electrical appliances taken into account are domestic lighting, freezer and refrigerator, a music installation, the iron and vacuum cleaner, a personal computer, a television, cooking appliances such as a hob, oven, microwave and kettle, a dishwasher, a tumble dryer and a washing machine. Figure 7 shows a profile with resulting electricity use and internal gains aggregated to a week for a single family. Internal gains can be lower or higher than the electricity consumption, depending on which appliance is consuming and the occurrence of internal gains from persons.

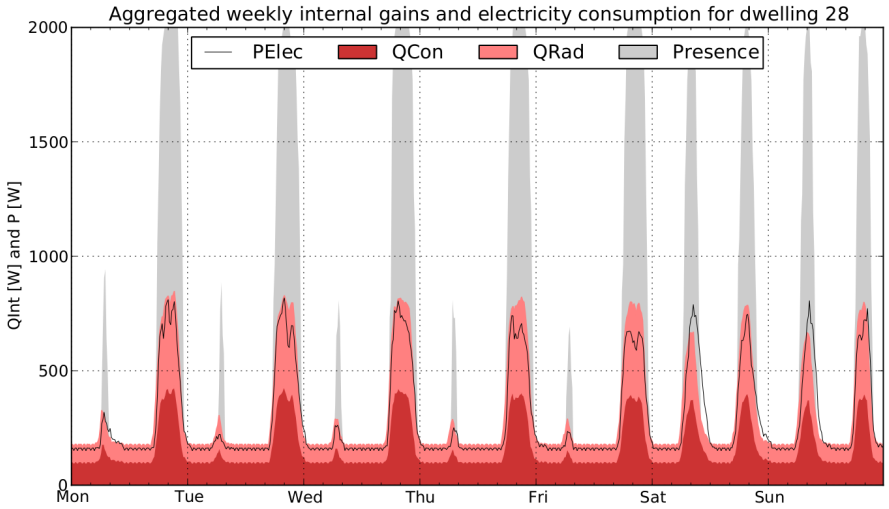


Figure 7. Aggregated weekly presence, internal gains and electricity consumption for a young couple both working full time during weekdays and partly present in the weekend (type (1)). $PElec$ = total electricity consumption without HVAC, $QCon$, $QRad$ = convective respective radiative heat gains. Presence is visualised as the proportion of maximum occupancy, presence during nights when the inhabitants are sleeping is not shown.

2.5.3 Domestic hot water

Special attention has been paid to a solid DHW model because of the increased fraction of the final energy demand for domestic hot water in low energy buildings. There are two important aspects in modelling DHW consumption in building simulation research: the tap profile and the total hot water consumption. Both aspects are discussed below.

The tap profile is strongly related to the activity of the building users, and therefore a stochastic model is needed for which each simulated dwelling shows a different consumption profile that is in accordance with the occupancy and activity of the users. Different stochastic models for the DHW tap profile can be found in the literature (Becker and Stogsdill, 1990; Fairey and Parker, 2004; Jordan and Vajen, 2001; Hendron and Burch, 2007; Widén et al., 2009). The approach within this work is based on the models of Jordan and Vajen (2001) and Widén et al. (2009).

Four different withdrawal categories have been defined, i.e. a short and medium withdrawal, a shower and a bath. For each category, the flow rate, total DHW volume and the average number of occurrences per day is fixed equal to Jordan and Vajen (2001). Ten-minute proclivities are determined based on the occupancy and activity proclivities from Richardson et al. (2010) for each category. The resulting stochastic profile for the DHW tap profile is achieved by discrete-time Markov chains based on a calibration scalar to end up with the desired average equivalent consumption per capita.

The total DHW consumption per capita depends on many parameters. Measurements and estimates made in several studies show a large variance in the results. In the following overview, all consumptions are converted to equivalent volumes at 60 °C, with cold water at 10 °C. A European SAVE study by Lechner (1998) reports an average consumption of 30 l/day per person with a range between 10 l/day and 80 l/day. Marsh (1996) computed a daily consumption for washing of only 14 l/day per person, but if (hot fill) dish and cloth washing are included, this number rises to 41 l/day per person. Widén et al. (2009) used two Swedish measurement campaigns with the following consumptions: about 40 l/day per person for detached houses and between 51 l/day and 154 l/day per person for appartments. Several measurement campaigns followed up by 3E in Belgium have resulted in an average of 30 l/day per person for multi-family houses.

Due to the detailed stochastic model, the average daily DHW consumption is rather an output than an input. For the whole neighbourhood, with 82 residents, the average amounts to 33.1 l/day per person at 60 °C. This consumption is imposed at the flange of the storage tank. Consequently, distribution losses are neglected in this study. An aggregated weekly tap profile for a family of type (4) is shown in Figure 8.

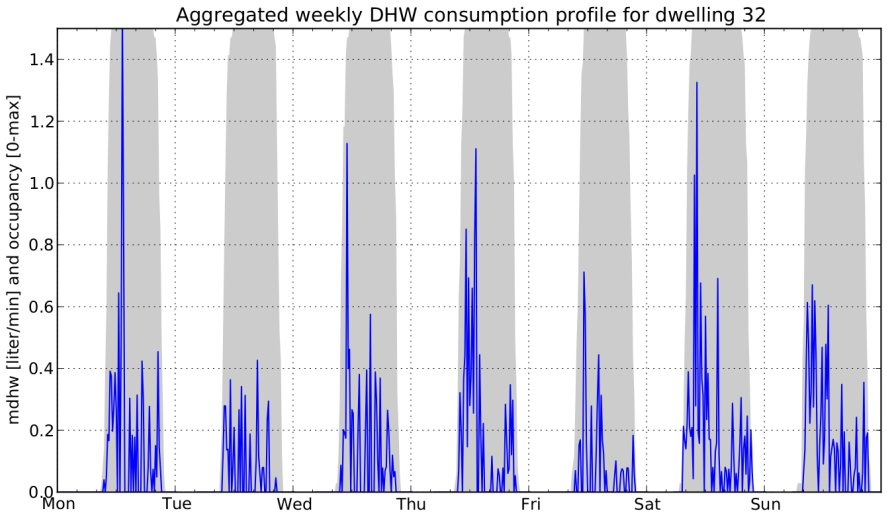


Figure 8. Aggregated weekly presence and DHW consumption for a retired couple (type (4)). Presence is visualised as the proportion of maximum occupancy, presence during nights when the inhabitants are sleeping is not shown.

2.6 Neighbourhood

The dwellings are connected to a low voltage distribution grid, shown in Figure 11 (b) (on page 15). The same IEEE 34 node grid topology is used as in Baetens et al. (2012), and sizing is according to the *medium feeder strength*, which stands for aluminium cables with sections of 95 mm^2, 50 mm^2 and 35 mm^2 for the different lines. The different household types are distributed randomly over the neighbourhood.

Table 2. Overview of model parameters

Symbol	Parameter	Value
Dwelling		
A_{heat}/V_{heat}	Heated floor surface and volume	196 m^2 / 643 m^3
$\dot{V}_{inf}$	Infiltration flow rate	0.03 ACH
$\dot{V}_{ven}$	Ventilation flow rate	0.5 ACH
η_{hr}	Ventilation heat recovery efficiency	0.84
UA_{tot}	Overall heat loss coefficient (incl. infiltration and ventilation with heat recovery)	106 W/K
Φ_{design}	Specific building design heat load (Ukkel, Belgium)	15.8 W/m^2
g_s	Solar transmittance of the solar shading	0.24
$ctrl_s$	Irradiance thresholds for automatic control of solar shading (down - up)	250 - 150 W/m^2
Heating		
$Q_{hp,nom}$	Nominal power of the HP at 2/35 and 2/45 °C	3459 / 3169 W
COP_{hp}	COP of the HP at 2/35 and 2/45 °C	3.17 / 2.45
m_{hp}	Water content of heat pump condenser	10.0 l
UA_{hp}	Transmission losses of heat pump	12.9 W/K
m_{hydr} [a]	Total water content of hydronic heating system (excl. HP, FH and DHW tank)	4.0 l
UA_{hydr} [a]	Total transmission losses of hydronic system (excl. HP, FH and DHW tank)	8.0 W/K
$T_{fh,design}$	Temperature regime floor heating at −8 °C outside	35/30 °C
$TSet_{DHW}$ [b]	Set temperature in DHW storage tank	53 °C
DHW storage tank		
V	Volume	0.3 / 0.5 m^3
H	Height	1.4 m
N_{nodes}	Number of nodes (node 1 is top node)	10
U_{ins}	Transmission losses through insulation	0.4 W/(m^2 K)
UA_{fix}	Additional transmission losses (independent of tank volume)	1.61 W/K
A_{hx}	Surface of internal heat exchanger (coil)	4.1 m^2
Pos_{hx}	Position of the coil (upper tank node - lower tank node)	$4-10$
h_{in}	Convective heat transfer coefficient at inside of coil	4000 W/(m^2 K)
h_{con}	Conduction heat transfer coefficient through coil	3300 W/(m^2 K)
h_{out}	Convective heat transfer coefficient at outside of coil	867 W/(m^2 K)

[a] Combination of different pipes and pumps which can be at different temperatures.

[b] According to a temperature sensor in the second tank node. This set temperature is increased at periods of load shifting in the different DSM strategies in order to start charging the DHW tank. $TSet_{DHW}$ is *never* lower than 53 °C.

2.7 Parameter overview

An overview of the parameters used for the different submodels is given in Table 2.

3. Reference case

3.1 Thermal comfort

With identical buildings and control, the thermal comfort and heat demand depend only on the user behaviour (presence and appliance use). Figure 9 shows that both winter and summer comfort are satisfied for the dwellings with lowest and highest internal gains.

The DHW comfort is calculated as the mass flow rate that is withdrawn at temperatures above 40 °C divided by the total DHW consumption. The mixing valve has a set point of 45 °C. Due to the way the stochastic DHW draw profiles are calculated, every dwelling has a limited number of days during which the total DHW load is very high. Therefore, the DHW comfort varies between 96.4 % and 99.8 % as shown in Figure 10.

3.2 Energy use

Figure 10 gives an overview of the energy use, SPF of the heat pump, primary energy efficiency of the total heating and DHW system and DHW comfort. Despite the low energy standard, the heat demand is predominantly caused by space heating. This is due to the relatively low DHW

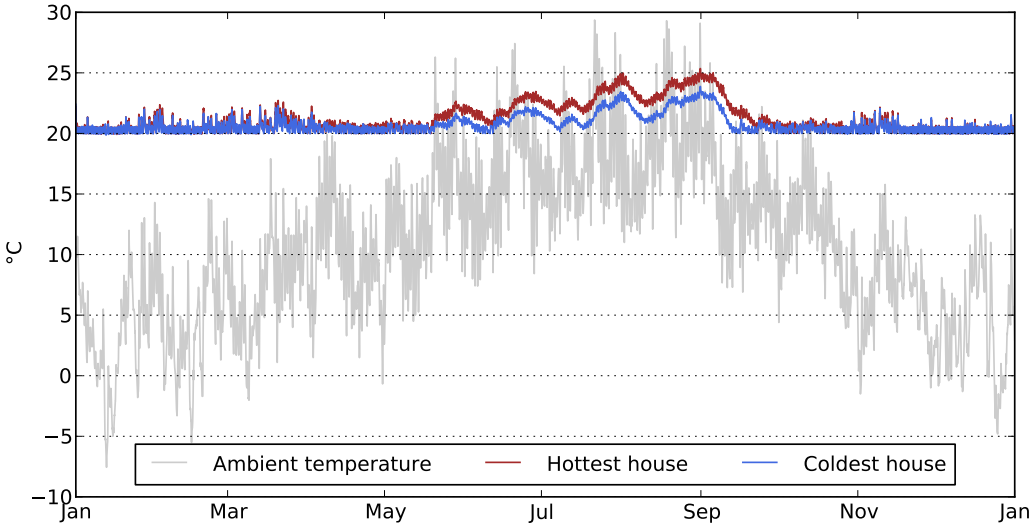


Figure 9. Ambient temperature and operative temperature in the hottest and coldest dwelling

demand profiles and the conservative settings of the automatic solar shading devices. The SPF of the heat pump and the total primary energy efficiency are within acceptable ranges. Taking into account a primary energy factor of 2.5 for electricity, we see that the primary energy efficiency is lower than the SPF of the heat pump. This is due to thermal losses in the storage tank and hydronic circuit. The required nominal power of the PV arrays in order to reach a yearly zero energy balance lies between 5.0 kW and 7.5 kW peak power.

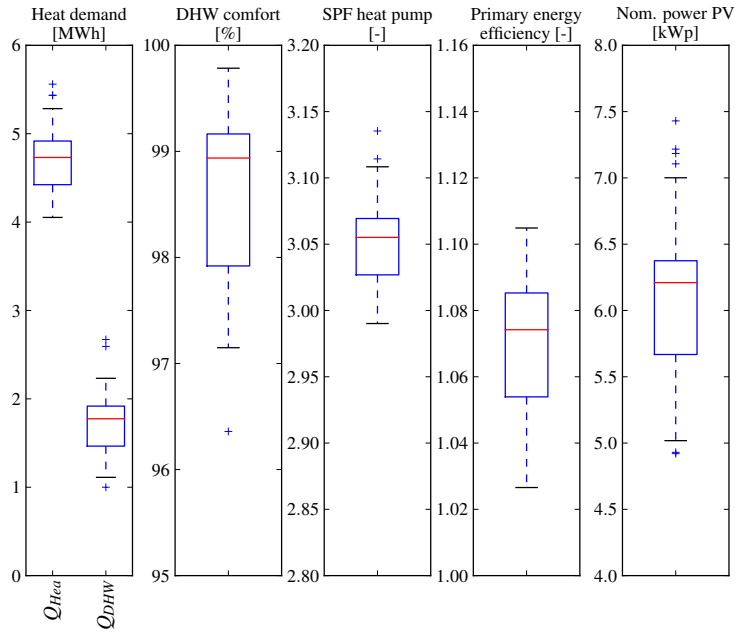
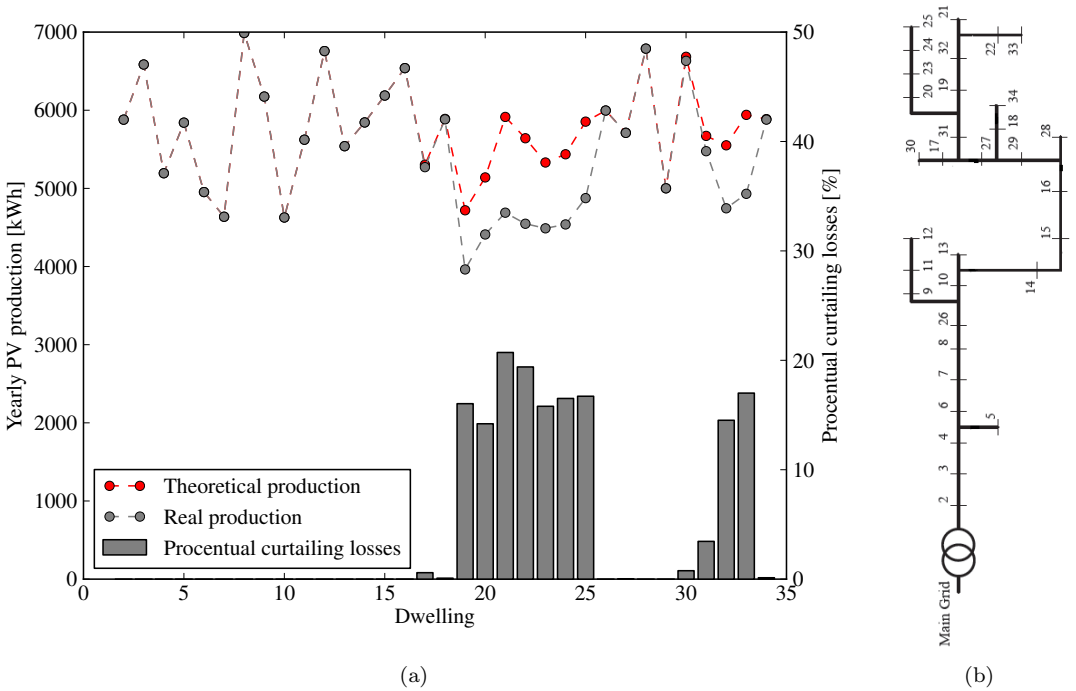


Figure 10. Box plots showing the median and quartile range of indicated variables for the 33 dwellings in the reference case. Outliers (values outside of 1.5 × quartile value) are presented by '+'



(a) (b)

Figure 11. a) Yearly inverter shut-down losses for dwellings according to numbering in grid topology b) .

3.3 Energy balance

Figure 11 shows that inverter shut-down is only affecting 10 out of the 33 dwellings. The shut-down losses can reach up to 20 % of annual PV production of these systems. The losses depend on the position of the dwelling in the grid and the figure shows that the weak branches are those who are furthest away from the transformer.

The net yearly electricity consumption of the neighbourhood E_{NBH} would be $-1.8\,\mathrm{MWh/a}$ in case of an ideal feeder. This means that the neighbourhood would be a net electricity producer on a yearly basis due to slight oversizing of the PV systems. However, due to ohmic grid losses and inverter shut-down, the small yearly overproduction becomes a net consumption of 12.4 MWh/a. Compared to the electricity use of the dwellings, the ohmic losses amount to 3.0 % and the inverter shut-down losses are 4.6 % of the yearly demand. This may seem relatively low, specifically when compared to results of Baetens et al. (2012). For a similar case, Baetens *et al.* found curtailing losses of 22 % and ohmic losses of 1.9 %. The difference in curtailing losses is entirely due to changed regulations: in the model of Baetens *et al.*, the inverters were configured to shut-down at a voltage deviation of 6 %, i.e. 243.8 V, but in the mean time this legislation has been harmonized with EN 50438:2007 and since medio 2012 the limit is fixed at 10 % voltage increase, i.e. 253.0 V (SynerGrid, 2012). The increase in ohmic losses is due to the higher total consumption and installed PV power in the considered neighbourhood.

3.4 Aggregated power profiles

In order to get a better understanding of the phasing between average PV production and the electricity consumption we have aggregated the different power profiles in Figure 12 (upper left). This figure shows the aggregated daily power for user electricity consumption, PV production and HP operation for dwelling 19 which has about 17 % of curtailing losses. The aggregation is done for the whole year, including days without curtailing.

As Figure 12 (upper left) shows, in dwelling 19, the electricity consumption of appliances and lighting has a morning and evening peak. The heat pump also operates most in the morning

and evening, with a time shift of about two hours (later) compared to the user electricity consumption. This can be explained by the morning and evening peaks in water consumption and the presence of a DHW storage tank causing the HP to reheat the tank after most DHW withdrawals. As a result, the electricity consumption is not well in line with the electricity generation profile of the PV system. Curtailing typically takes place between 10h-16h.

4. Demand side management

4.1 Rule-based control strategies

The challenge tackled in this paper is to adapt the control of the DHW production in order to reduce the net yearly electricity consumption of the neighbourhood E_{NBH}. Given the ohmic grid losses, E_{NBH} will never become zero without increasing the PV capacity compared to the reference case, even though most control strategies can reduce the ohmic losses to a small extent.

As mentioned before, reducing curtailing losses is straightforward: if the local consumption is increased sufficiently at periods of high grid voltage, the PV inverters will not shut down. This could however increase E_{NBH} instead of decreasing it. Therefore, the aim is not to reduce curtailing losses but E_{NBH}.

The control strategies are divided in three different categories based on the trigger used to initiate the load shifting. These triggers can be a clock, the power exchange with the grid or the voltage. When the trigger is activated, the temperature set point in the DHW storage tank $TSet_{DHW}$ is increased. The amount of the temperature increase is a parameter of the control and will be varied in the analysis. Some additional variants have been defined as shown in Table 3. Only rule-based control strategies are considered in this paper. Comparing rule-based DSM with full neighbourhood optimal control could be the topic of future research.

For reference: the simulations were executed on desktop computers with two different cpu's (Intel Xeon(R) at 2.53 GHz and at 3.07 GHz) and depending on the cpu and (primarily) the control strategy the simulation time was between 1.2 and 4.3 days for simulating one year.

4.2 Load shifting

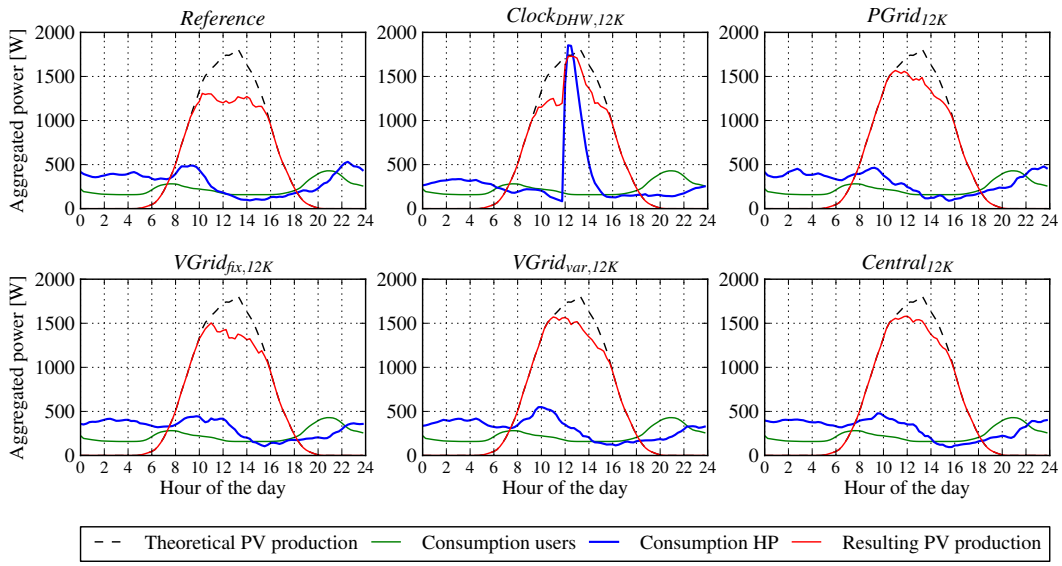


Figure 12. Aggregated power density profiles for dwelling 19 with a DHW storage tank of 0.3 m^3.

Table 3. Overview of DSM control strategies

Name	Trigger for DSM	Details	Implementation effort
$Clock_{DHW}$	Clock	Between 12h00 and 16h00, $TSet_{DHW}$ is increased.	Very low, no sensors required.
PGrid	Power exchange of the dwelling with the grid	When the power injection in the grid surpasses P_{lim}, $TSet_{DHW}$ is increased. P_{lim} is the same regardless PV sizing.	Moderate. Requires power measurement, preferentially based on inverter output before curtailing and without HP consumption to avoid unstable control or the need for large hysteresis.
$VGrid_{fix}$	Voltage at dwelling's grid connection	When the voltage surpasses V_{lim}, $TSet_{DHW}$ is increased. V_{lim} is the same for all dwellings and is typically a few Volt lower than 253 V [a].	Low, only requires a single voltage measurement.
$VGrid_{var}$	Voltage at dwelling's grid connection	When the voltage surpasses V_{lim}, $TSet_{DHW}$ is increased. V_{lim} depends on the position of the dwelling in the grid.	Low on building side, only requires a single voltage measurement. Power flow calculation required once in order to determine V_{lim} for each dwelling.
Central	Voltage at dwelling's grid connection and temperature of DHW tank.	A central intelligence is present with access to the voltage and temperature of the DHW tank in each dwelling. When somewhere in the grid V_{lim} is exceeded, $TSet_{DHW}$ of the DHW tank with lowest temperature is increased, regardless of the position of that dwelling in the grid.	High. Requires centralised monitoring and control and can conflict with privacy of the occupants.

[a] In all simulations with $VGrid_{fix}$, V_{lim} has been set to 251 V, 2 V lower than the shut-down limit to create a safety margin.

[b] The power flow calculation imposes an equal load to all dwellings for which the maximum voltage in the grid reaches 251 V. The corresponding voltage at each connection point is V_{lim}.

A first strategy for shifting the HP operation is a clock-based increase of $TSet_{DHW}$. To keep this DSM control very simple, the temperature is increased at the same time (12h-16h) in *every* house on *all* days of the year, even when there is no curtailing risk at that moment or position in the grid. The aggregated power profiles for $Clock_{DHW,12K}$, with a daily temperature increase of 12 K is shown in Figure 12 (upper middle). We can see a clear shift in the operation of the heat pump with a very sharp peak at 12h. As a consequence, the morning and evening peaks are largely flattened. The result is a strong reduction of inverter shut-down between 12h and 14h. The effect does not last till 16h as the heat pumps in the neighbourhood switch off one by one when the temperature in their respective storage tank reaches the increased $TSet_{DHW}$.

The voltage increase in the grid is caused by simultaneous injection of surplus electricity by all dwellings. When we try to increase the self-consumption γ_S at times of high injection power we expect the curtailing losses to decrease. Figure 12 (upper right) shows the effect of $PGrid_{12K}$. The shift of HP operation is much less pronounced as for $Clock_{DHW,12K}$. This is because this DSM control is only active on sunny days and the aggregated profile is computed based on all days of the year. Nevertheless, the impact on curtailing losses is high, specifically in the morning. In the afternoon, when the storage tanks in the neighbourhood start reaching the increased $TSet_{DHW}$, the effect is lower. It has to be noted that in this control strategy, *all* dwellings participate, even if they do not suffer from inverter shut-down. As the trigger for DSM is a fixed and identical P_{lim} for all dwellings, this control will be activated more often for large PV systems.

The reason for inverter shut-down being excessive voltage, it seems more logic to base the DSM strategy on a measurement of the voltage at the dwelling's grid connection. There are two options for setting the voltage limit V_{lim} at which $TSet_{DHW}$ is increased. In the $VGrid_{fix}$ strategy, P_{lim} is the same for all dwellings (251 V). In $VGrid_{var}$, P_{lim} depends on the position of the dwelling and the characteristics of the feeder. The idea is to activate the control in the

dwellings when based on their own voltage measurement there is a good reason to suspect that curtailing is about to happen somewhere else. The effect on the aggregated power for both controls with a $\Delta TSet_{DHW}$ of 12 K is shown in Figure 12 (lower left and middle). The impact of sharing the burden among all dwellings can clearly be seen: $VGrid_{var,12K}$ reduces the curtailing losses more than $VGrid_{fix,12K}$.

A more advanced DSM control based on V_{lim} requires a central management system that has access to all voltages in the grid and the temperatures in the DHW tanks and that can increase $TSet_{DHW}$. This way, the controller can select which HP is to start to avoid curtailing. Ideally, the controller would take into account the grid topology and select the dwelling(s) that will have most effect on the anticipated problem. However, the *Central* control investigated in this paper only selects based on storage tank temperature. With a maximum $\Delta TSet_{DHW}$ of 12 K, the resulting aggregated power is shown in Figure 12 (lower right). The *Central* strategy is clearly more complicated and expensive than all other studied controls as it requires a central system for monitoring and control. However, it is still much easier (and cheaper) than model predictive control (MPC) as it does not require weather and user behaviour forecasts, system models and an optimisation framework.

4.3 Resulting net yearly electricity consumption

So far, we have only discussed the load shifting behaviour of the DSM control strategies and the resulting reduction in curtailing for a single case (dwelling 19). In this section we also consider the effects of the higher average storage tank temperature and shifted heat pump operation on the total net electricity consumption of the neighbourhood, E_{NBH}. We define the net electricity savings as $\Delta E_{\mathrm{NBH}} = E_{\mathrm{NBH,\ DSM}} - E_{\mathrm{NBH,\ ref}}$. Figure 13 shows the *loss-benefit space* for the neighbourhood. In this graph, every marker is the final result of a control strategy on neighbourhood level. The number in the marker is the increase in $TSet_{DHW}$ when the control is activated. The horizontal axis represents the relative electricity demand compared to the reference case. The vertical axis shows the relative curtailing and ohmic losses compared to the reference. Therefore, the reference lies in the origin, and a case for which gains and savings are equal would lie on the *status quo line*, the diagonal through the origin. The resulting net savings for every case ΔE_{NBH}, is the difference between relative savings and relative consumption and is represented by the vertical distance of the marker to the status quo line.

A first remarkable result is the good performance of the most simple control strategy, $Clock_{DHW,4K}$. It is the only control for which the electricity demand is substantially lower than the reference case −3.4 MWh, and at the same time it is able to reduce curtailing losses by 2.3 MWh. These effects add together and result in ΔE_{NBH} of 5.6 MWh. As a matter of fact, no single other control strategy can do better. Variants of $Clock_{DHWK}$ with $\Delta TSet_{DHW}$ equal to 8 K or 12 K are much less interesting. They can reduce the curtailing losses a little bit further, but the savings on electricity demand completely vanish. The reason why $Clock_{DHW,4K}$ outperforms all other strategies is the fact that besides reducing curtailing losses on sunny days, it also has a benefit during almost all other days. As pointed out earlier by De Coninck et al. (2010), the timed increase of $TSet_{DHW}$ shifts the operation of the air-to-water HP to the afternoon, when the ambient temperature is often a few degrees higher than in the morning or evening. As long as $\Delta TSet_{DHW}$ is low, this effect outweighs the performance loss due to the increased condenser temperature and the additional thermal losses in the TES tank and hydronic circuit. This is confirmed by the median of the HP's SPF for all dwellings: it rises from 3.06 in the reference case to 3.17 for $Clock_{DHW,4K}$.

Furthermore, when the tank temperature is temporarily increased, the top of the tank will still be warm enough after the next DHW withdrawal and the tank does not have to be reheated as soon as in the reference case. This will improve the stratification in the tank and lead to the following benefits:

- less heat pump cycles, resulting in lower thermal losses of the heat pump and hydronic

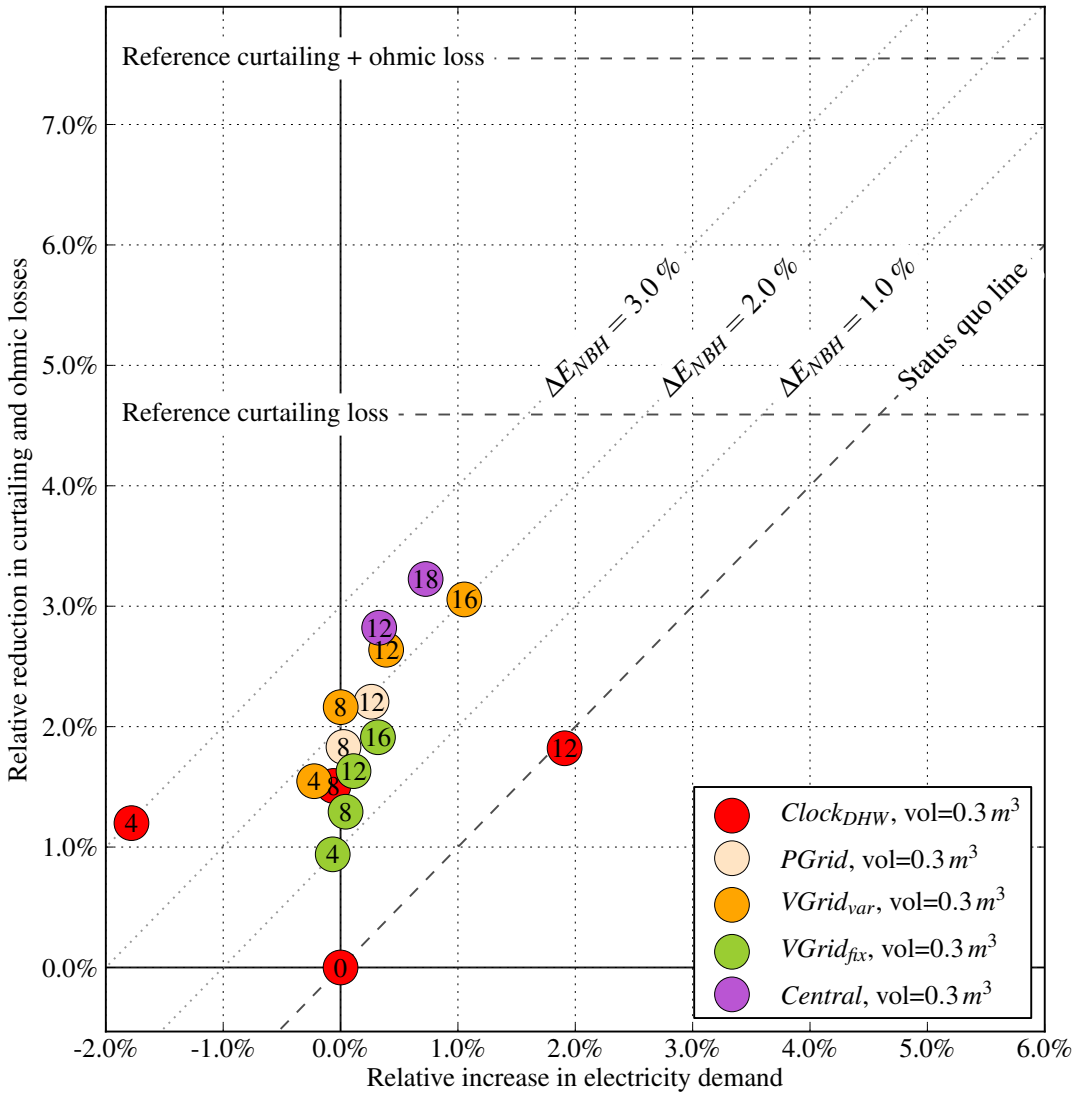


Figure 13. Loss-benefit space for rule-based DSM with 0.3 m^3 DHW storage tank.

circuit

- lower condenser temperatures at the start of the next tank heating cycle, resulting in a higher SPF
- lower average temperatures at the bottom and middle of the tank, resulting in lower thermal losses for these layers.

The cumulative result of these effects is a reduction of total thermal losses for the entire neighbourhood of 4.2 MWh (= 8.5 %). Of course, the other strategies benefit from similar effects, but only during the sunny periods when their DSM strategy is activated. This means that all other strategies can be combined with $Clock_{DHW,4K}$ in order to try to combine the benefits from both strategies. Some results of combined strategies are discussed in section 4.5.

Figure 13 also shows the results for the other strategies for different values of $\Delta TSet_{DHW}$. We see that for all strategies, both electricity demand and reduction of curtailing losses increase

with rising values of $\Delta TSet_{DHW}$. Therefore, the net neighbourhood savings, ΔE_{NBH} tend to show a maximum as a function of $\Delta TSet_{DHW}$. Sometimes the maximum does not seem to be reached because simulations with temperature increases of more than 18 K are not performed to stay within the validity range of the heat pump model.

There is a clear rank in the performance of the control strategies. We put them in order of decreasing effectiveness (based on ΔE_{NBH}) , and indicate which $\Delta TSet_{DHW}$ gives the best result:

(1) $Clock_{DHW}$, optimal $\Delta TSet_{DHW} = 4\,\mathrm{K}$
(2) *Central*, optimal $\Delta TSet_{DHW} = 12\,\mathrm{K}$ and $18\,\mathrm{K}$
(3) $VGrid_{var}$, optimal $\Delta TSet_{DHW} = 12\,\mathrm{K}$
(4) *PGrid*, optimal $\Delta TSet_{DHW} = 12\,\mathrm{K}$
(5) $VGrid_{fix}$, optimal $\Delta TSet_{DHW} = 16\,\mathrm{K}$.

Overall, we can conclude that for a $0.3\,\mathrm{m}^3$ storage tank and with the proper $\Delta TSet_{DHW}$, these rule-based control strategies are able to reduce E_{NBH} by 3.0 MWh to 5.6 MWh. This corresponds to a reduction of curtailing losses by 35 % to 65 %. Compared to the total electricity demand of the neighbourhood (without taking into account PV production), these savings represent 1.6 % to 3.0 %.

4.4 Effect of increased storage tank size

All results discussed so far were based on a DHW storage tank of $0.3\,\mathrm{m}^3$. It is clear that by increasing the volume of this tank, the system will be able to reduce the curtailing losses even more. However, the thermal losses will also be higher, and may overcompensate the benefits of additional load shifting. Figure 14 shows the results with a storage tank size of $0.5\,\mathrm{m}^3$. In this figure, also the reference case has this larger DHW tank. This does barely influence the reference curtailing losses, but increases the E_{NBH} of the reference case by 1.6 MWh.

As expected, all strategies are able to reduce the curtailing losses further than with a $0.3\,\mathrm{m}^3$ storage tank. The most notable change is a reduced performance of the $Clock_{DHW}$. Whereas for all other strategies, the position of the markers is very similar to the previous results, the markers of $Clock_{DHW}$ are clearly shifted to the right. This specifically means that the increased system performance of $Clock_{DHW,4K}$ is less pronounced with a larger storage tank. As a result, this strategy is outperformed by the more complicated control strategies $VGrid_{var}$ and *Central*.

The real merit of a larger storage tank has to be evaluated by comparison with the original reference case which has the smaller tank. This is done in Figure 15, where the reference case with DHW tank of $0.3\,\mathrm{m}^3$ is placed in the origin. In a first instance, we do not discuss the three markers at the end of the arrows (they will be discussed in the next section). From this figure we can clearly see the shift of all cases with a DHW tank of $0.5\,\mathrm{m}^3$ to the right and upwards (except for the reference). However, none of the cases with a larger storage tank is able to compensate the additional electricity demand by stronger reduction of curtailing losses. This brings us to an important conclusion of this study: with the simulated control strategies it does *not* make sense to install additional thermal energy storage to increase the DSM capabilities of the systems.

4.5 Combinations with $Clock_{DHW,4K}$

Finally, we want to combine the merits of the most simple strategy on the days *without* curtailing with the performance of the advanced strategies on the days *with* curtailing. This has been simulated for three cases and visualised with arrows in Figure 15.

The combinations are indeed an improvement of the original strategies. The improvement in energy efficiency is a little bit smaller than anticipated, but on the other hand there is even an additional reduction of curtailing losses. However, our previous conclusion holds: the systems with the smaller storage tank show a better energy performance.

The best results are obtained with the combination of $Clock_{DHW,4K}$ and $VGrid_{var,16K}$. This

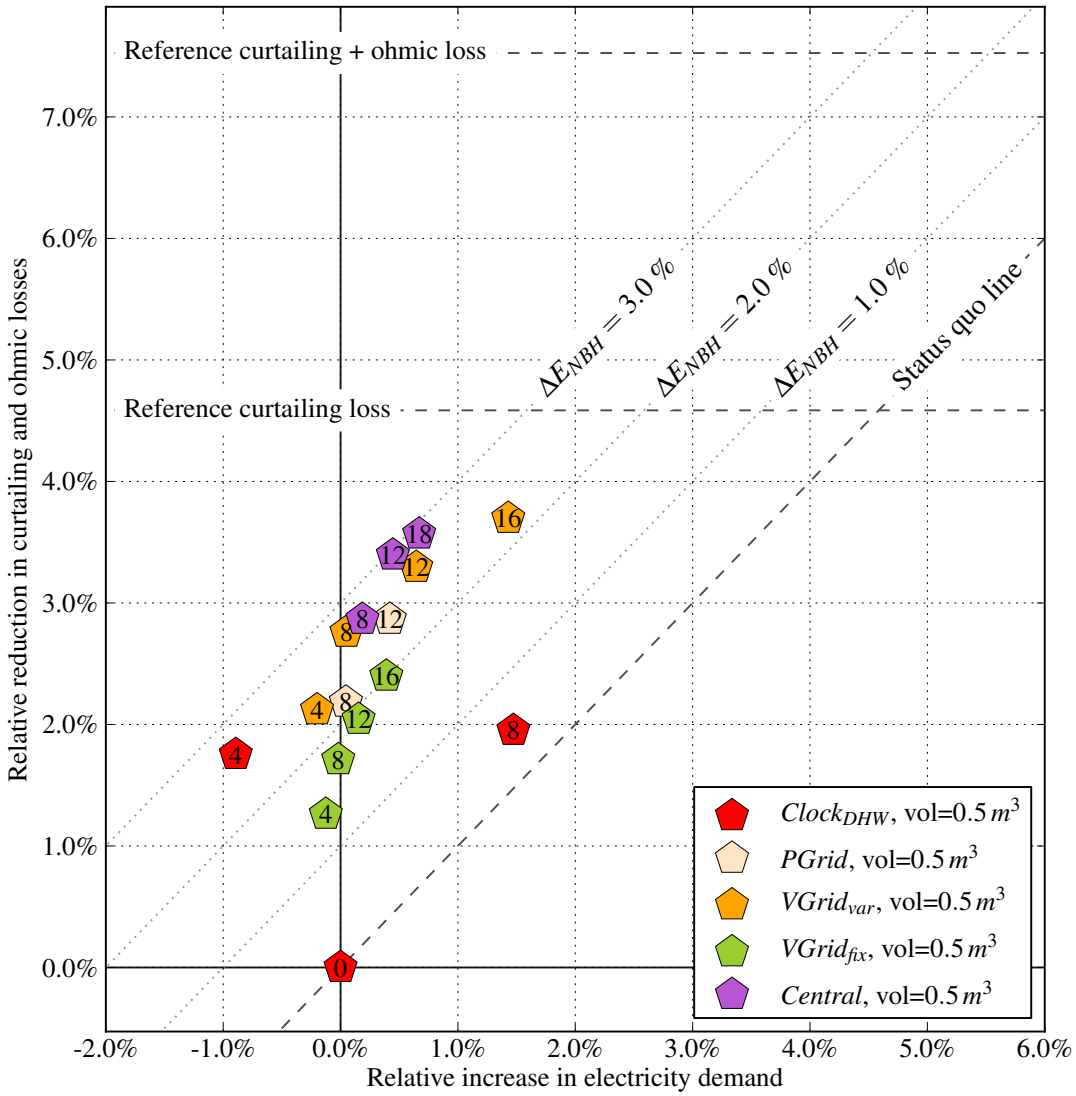


Figure 14. Loss-benefit space for rule-based DSM with 0.5 m^3 DHW storage tank.

simulation realised a ΔE_{NBH} of 6.4 MWh which corresponds to a reduction of curtailing losses by 74 % or a reduction of E_{NBH} by 3.4 %. We could have simulated more combinations and other values for $\Delta TSet_{DHW}$. For instance, from Figure 15 it can be anticipated that a combination of $Clock_{DHW,4K}$ with $VGrid_{var,12K}$ or $Central_{18K}$ will bring ΔE_{NBH} even higher. There are probably also other control strategies worth investigating. However, with the current results, we already show that simple rule-based controls are able to strongly reduce curtailing losses in low energy dwellings with a high PV penetration while decreasing the net electricity demand.

4.6 Load matching and grid interaction indicators

The aim of this study is to decrease the net electricity consumption of the neighbourhood E_{NBH} as a whole by avoiding PV inverter shut-down. Therefore, a neighbourhood model has been

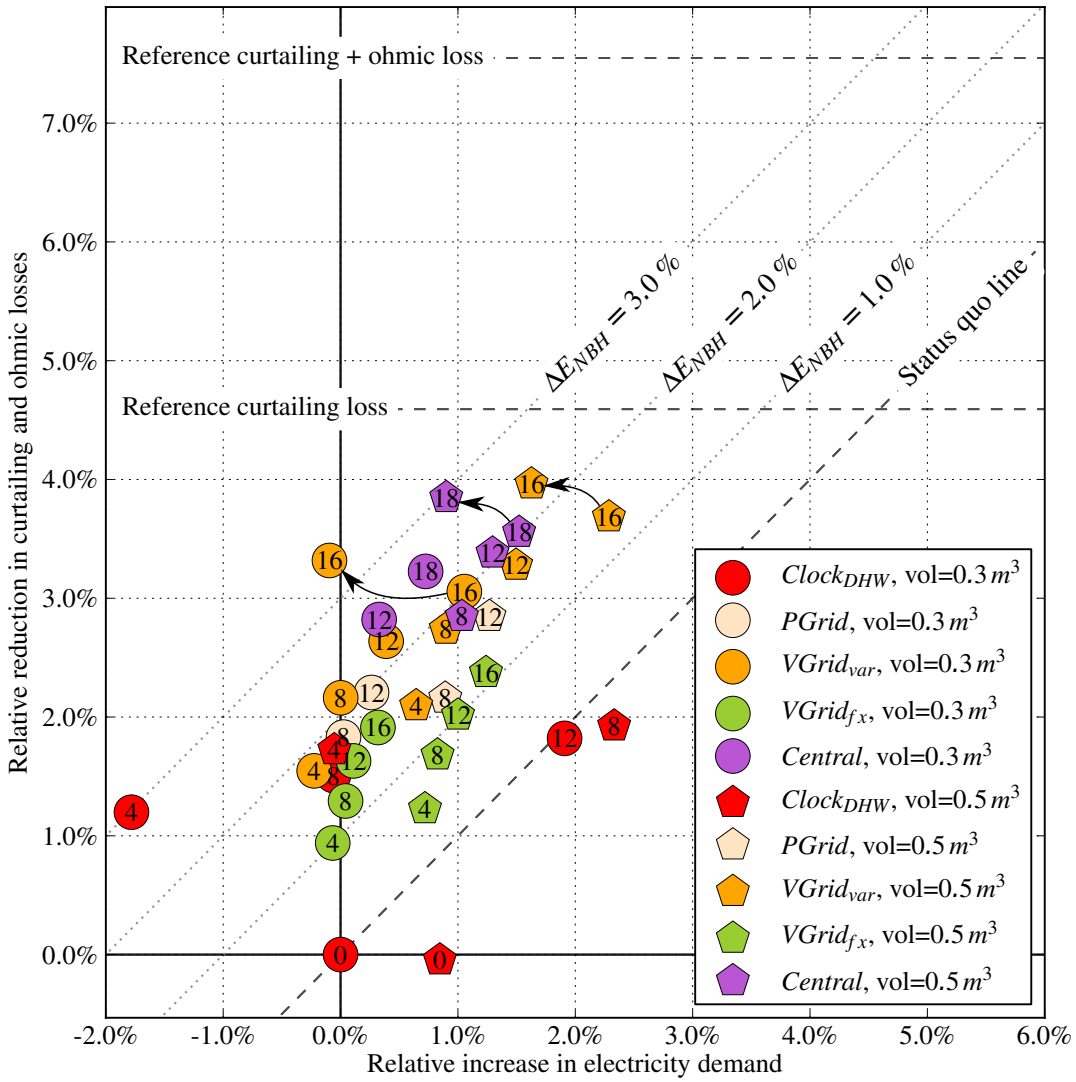


Figure 15. Loss-benefit space for rule-based DSM with 300 l and 500 l DHW storage tank. The three markers at the end of arrows are combinations of that control strategy with $Clock_{DHW,4K}$

developed in Modelica. When such a model is not available and the only tool at hand is a stand-alone building simulation program, the interaction of the building with the electricity grid can be characterized by load matching and grid impact (LMGI) indicators. LMGI indicators are defined by different authors (Salom et al., 2011; Verbruggen et al., 2011; Baetens et al., 2012) in order to quantify the balance between local electricity generation and consumption and the consequences of distributed generation on the electricity grid. In this section we will consider more specifically the self-consumption γ_S and self-generation γ_D, calculated as

$$\gamma_S = \frac{\int \min\{P_D, P_S\} dt}{\int P_S dt} \tag{7}$$

$$\gamma_D = \frac{\int \min\{P_D, P_S\} dt}{\int P_D dt} \tag{8}$$

where P_S is the local power supply (ie. PV production) and P_D the local power demand. The term $\min\{P_D, P_S\}$ represents the part of the power demand instantaneously covered by the local PV power supply or the part of the power supply covered by the demand (Baetens et al., 2012).

These indicators have to be used with caution because they are biased by bad control and inefficiency. For example, the operation of a heat pump at very high temperatures in order to store thermal energy during times of local overproduction of electricity will clearly increase the self-consumption. However, there is no guaranteed energy saving on total system level and/or reduction in greenhouse gas emissions. The very contrary can be true, as will be shown here.

A scatter plot of the average self-consumption and self-generation for all dwellings in the neighbourhood and for all investigated control strategies is shown in Figure 16. In this figure, both indicators are plotted as a function of the relative energy savings of the neighbourhood ΔE_{NBH}. This figure shows how biased these LMGI indicators can be. Although it is true that all efficient strategies have high indicators, the opposite is *not* true: a high indicator does not imply a high energy efficiency. As an example, we can consider the points in the left upper corner of the figure: these cases have a higher self-consumption and self-generation than the reference case, but result in an increased electricity consumption of the neighbourhood. In order to save energy, it should therefore *never* be the aim to increase the self-consumption of individual buildings as such.

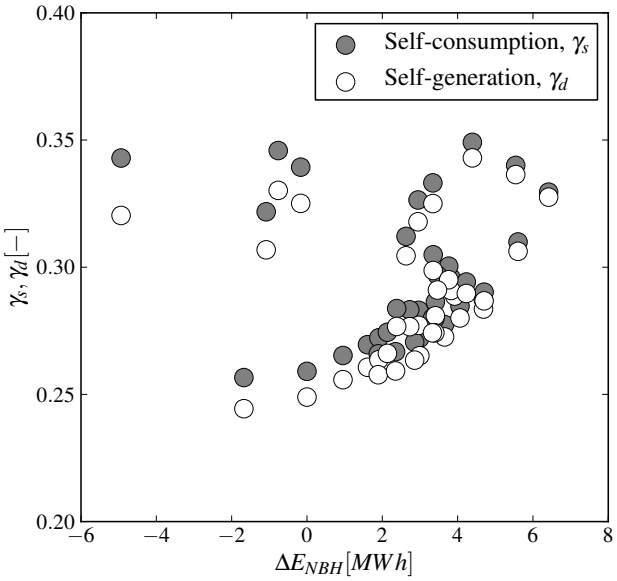


Figure 16. Scatter plot of average self-consumption and self-generation for all control strategies versus ΔE_{NBH}

This reasoning can be extended to neighbourhoods, districts, countries. As long as the studied system is interfaced with other consumers and production units which are not included in the model, side-effects on the global scale occur and conclusions on global system level have to be drawn with care. Sometimes such conclusions are simply not valid. It is therefore *not* the aim to increase the self-consumption of the neighbourhood as a whole.

5. Summary and conclusions

We have presented an integrated bottom-up approach to model and simulate neighbourhoods with Modelica. The model includes multiple single-family dwellings and the low voltage grid to which they are connected. For each of the dwellings, the model incorporates a thermal building model, HVAC system with DHW storage tank, air-to-water heat pump and floor heating, and a fully stochastic user behaviour model for presence, appliances, lighting and DHW use.

The model is used to study inverter curtailing losses in a low energy neighbourhood with 33 dwellings with a high total installed PV power. In the reference case, inverter shut-down causes an electricity generation loss of 8.6 MWh or 4.6 % of the initial electricity demand of the neighbourhood. A first conclusion is that these losses are much lower than previously reported results under similar circumstances. The reason can be found in changed regulations, allowing voltage deviations in the distribution grid of up to 10 % instead of 6 % previously.

In order to reduce this loss, different rule-based DSM strategies applied to the DHW production are proposed and simulated, both for a 0.3 m^3 and 0.5 m^3 DHW tank. Different conclusions are drawn from the results.

- The curtailing losses can be reduced to a large extent by different rule-based control strategies. However, the net energy saving is generally smaller than the reduction in curtailing losses because of increased thermal losses.
- The simulated controls realise *net* savings of up to 74 % of the original curtailing losses. This corresponds to a reduction of the electricity demand of the total neighbourhood (without taking PV generation into account) by 3.4 %.
- Rule-based control strategies can be very straightforward. The most simple one, $Clock_{DHW,4K}$, is just a timed increase of the set temperature in the storage tank and is difficult to beat. The most advanced control under investigation, *Central* brings only limited additional energy savings compared to $VGrid_{var}$.
- The best results are obtained when the whole neighbourhood participates in the load shifting, including dwellings that never experience curtailing. This can be accomplished when the trigger for DSM is a (fixed) injection power or a dwelling-dependent voltage limit (which leads to better results).
- Load matching and grid interaction indicators must be used with care. Both the very effective and ineffective control strategies can have a high self-consumption γ_s and self-generation γ_d. This result can be generalized: it is often not possible to draw valid conclusions on a global scale from a model of a local system.
- Increasing the DHW storage size from 0.3 m^3 to 0.5 m^3 always results in a higher electricity consumption, regardless of the control strategy used.

This study shows that even with small TES tanks and very simple controls, PV inverter shut-down can strongly be reduced. Model predictive control strategies are *expected* to lead to better results. However, they require significantly higher investments which may not be compensated by additional savings. Future research has to concentrate on the window of improvement by MPC over the already successful rule-based controls.

6. Acknowledgement

The authors gratefully acknowledge the KU Leuven Energy Institute (EI) for funding this research through granting the project entitled *Optimized energy networks for buildings* and the European Commission for granting the *Performance Plus* project in the 7^{th} Framework Programme.

References

Ackermann, T. and V. Knyazkin (2002). Interaction between distributed generation and the distribution network: operation aspects. In *IEEE/PES Transmission and Distribution Conference and Exhibition*, Volume 2, pp. 1357–1362.

Baetens, R., R. De Coninck, J. Van Roy, B. Verbruggen, J. Driesen, L. Helsen, and D. Saelens (2012). Assessing electrical bottlenecks at feeder level for residential net zero-energy buildings by integrated system simulation. *Applied Energy 96*(Special issue on Smart Grids, Renewable Energy Integration, and Climate Change Mitigation - Future Electric Energy Systems), 74–83.

Becker, B. and K. Stogsdill (1990). Development of Hot Water Use Data Base. In *ASHRAE Transactions*, Volume 96, Atlanta, GA, pp. 422–427. American Society of Heating, Refrigerating and Air Conditioning Engineers.

Bletterie, B., A. Gorsek, B. Uljanic, A. Woyte, T. Vu Van, F. Truyens, and J. Jahn (2010). Enhancement of the Network Hosting CapacityClearing Space for/with PV. In *European Photovoltaic Solar Energy Conference*.

Caamaño Martin, E., H. Laukamp, M. Jantsch, T. Erge, J. Thornycroft, H. De Moor, S. Cobben, D. Suna, and B. Gaiddon (2008). Interaction Between Photovoltaic Distributed Generation and Electricity Networks. *Progress in photovoltaics: research and applications 16*(7), 629–643.

Cheng, V. and K. Steemers (2011). Modelling domestic energy consumption at district scale: A tool to support national and local energy policies. *Environmental Modelling & Software 26*, 1186–1198.

Daikin Europe N.V. (2006). *Technical data Altherma ERYQ007A, EKHB007A / EKHBX007A, EKSWW150-300*. Oostende.

De Brabandere, K., A. Woyte, R. Belmans, and J. Nijs (2004). Prevention of inverter voltage tripping in high density PV grids. In *19th EU-PVSEC, Paris*, Number June, pp. 4–7.

De Coninck, R., R. Baetens, B. Verbruggen, J. Driesen, D. Saelens, and L. Helsen (2010). Modelling and simulation of a grid connected photovoltaic heat pump system with thermal energy storage using Modelica. In P. Andre, S. Bertagnolio, and V. Lemort (Eds.), *8th International Conference on System Simulation in Buildings (SSB2010)*, Number June, Liège, pp. P177.

De Soto, W., S. A. Klein, and W. A. Beckman (2006, January). Improvement and validation of a model for photovoltaic array performance. *Solar Energy 80*(1), 78–88.

Dugan, R. and T. McDermott (2001). Operating conflicts for distributed generation on distribution systems. In *Proceedings of the 45th Rural Electric Power Conference*, Little Rock, AR, USA, pp. A3/1–A3/6. IEEE.

EPIA (2012). Global market outlook for photovoltaics until 2016. (EPIA).

European Parliament (2010). Directive 2010/31/EU on the energy performance of buildings (recast). pp. 13–35.

Fairey, P. and D. Parker (2004). *A Review of Hot Water Draw Profiles Used in Performance Analysis of Residential Domestic Hot Water Systems*. Florida Solar Energy Center.

FOD Economie (2008). Bevolking - Private, grootte en collectieve huishoudens. Technical Report http://tinyurl.com/y8o662r (accessed on 22 January 2013).

Haller, M. Y., C. a. Cruickshank, W. Streicher, S. J. Harrison, E. Andersen, and S. Furbo (2009, October). Methods to determine stratification efficiency of thermal energy storage processes Review and theoretical comparison. *Solar Energy 83*(10), 1847–1860.

Han, Y., R. Wang, and Y. Dai (2009, June). Thermal stratification within the water tank. *Renewable and Sustainable Energy Reviews 13*(5), 1014–1026.

Hastings, S. (2004, April). Breaking the heating barrier. *Energy and Buildings 36*(4), 373–380.

Hendron, R. and J. Burch (2007). Development of standardized domestic hot water event schedules for residential buildings. In *Energy Sustainability 2007*, Number August.

Jordan, U. and K. Vajen (2001). *Realistic Domestic Hot-Water Profiles in Different Time Scales*. Marburg.

Kersting, W. (2001). Radial distribution test feeders. *IEEE Power Engineering Society Winter Meeting, 2001* (C), 908–912.

Kleinbach, E., W. Beckman, and S. Klein (1993, February). Performance study of one-dimensional models for stratified thermal storage tanks. *Solar Energy 50*(2), 155–166.

Lechner, H. (1998). *Analysis of Energy Efficiency of Domestic Electric Storage Water Heaters*. Study for the Directorate General for Energy (DGXVII) of the Commission of the European Communities Contract No. SAVE-4.1031/E/95-013.

Loga, T., N. Diefenbach, C. Balaras, E. Dascalaki, M. S. Zavrl, A. Rakuscek, V. Corrado, S. Corgnati, H. Despretz, C. Roarty, M. Hanratty, B. Sheldrik, W. Cyx, M. Popiolek, J. Kwiatowski, M. GroB, C. Spitzbart, Z. Georgiev, S. Lakimova, T. Vimmr, K. B. Wittchen, and J. Kragh (2009). Use of building typologies for energy performance assessment of national building stocks. Existent experiences in European countries and common approach. Technical Report June 2009, First TABULA Synthesis report.

Manfren, M., P. Caputo, and G. Costa (2011). Paradigm shift in urban energy systems through distributed generation : Methods and models. *Applied Energy 88*(4), 1032–1048.

Marsh, R. (1996). *Sustainable housing design : an integrated approach*. Ph. D. thesis, University of Cambridge.

Mather, D., K. Hollands, and J. Wright (2002, July). Single- and multi-tank energy storage for solar heating systems: fundamentals. *Solar Energy 73*(1), 3–13.

Newton, B. (1995). *Modeling of Solar Storage Tanks*. Ph. D. thesis, University of Wisconsin-Madison.

Olesen, B. (2001). Control of floor heating and cooling systems. In *CLIMA-2000*, Number September, pp. 15–18.

Richardson, I., M. Thomson, D. Infield, and C. Clifford (2010, October). Domestic electricity use: A high-resolution energy demand model. *Energy and Buildings 42*(10), 1878–1887.

Richardson, I., M. Thomson, D. Infield, and A. Delahunty (2009). Domestic lighting: A high-resolution energy demand model. *Energy and Buildings 41*(7), 781–789.

Rosen, M. a., R. Tang, and I. Dincer (2004, February). Effect of stratification on energy and exergy capacities in thermal storage systems. *International Journal of Energy Research 28*(2), 177–193.

Salom, J., J. Widén, J. Candanedo, I. Sartori, K. Voss, and A. J. Marszal (2011). Understanding Net Zero Energy Buildings: Evaluation of load matching and grid interaction indicators. In *Proceedings of Building Simulation 2011*, Volume 6, Sydney, Australia, pp. 2514–2521.

Sanyo (2008). *HIP-230HDE1 photovoltaic module*. http://www.technosun.com/eu/downloads/search-documentation.php (accessed on 22 January 2013).

Sera, D., R. Teodorescu, and P. Rodriguez (2007). PV panel model based on datasheet values. *IEEE* (4), 2392–2396.

Stokes, M., M. Rylatt, and K. Lomas (2004). A simple model of domestic lighting demand. *Energy and Buildings 36*(2), 103–116.

SynerGrid (2012). *Specifieke technische voorschriften voor decentrale productie-installaties die in parallel werken met het distributienet*. (C10/11 - revisie 4 juni 2012).

Verbruggen, B., R. De Coninck, R. Baetens, D. Saelens, L. Helsen, and J. Driesen (2011). Grid impact indicators for active building simulation. In *Innovative Smart Grid Technologies (ISGT), 2011 IEEE PES*, Number 2, pp. 1–6. IEEE.

Viessmann (2011). *Vitocell- 100-V, 390 liter, Datenblatt*. http://tinyurl.com/cdpv8rr (accessed on 21 April 2013).

Wetter, M. (2009). Modelica Library for Building Heating, Ventilation and Air-Conditioning Systems. In *The 7th International Modelica Conference*, pp. 393–402. The Modelica Association.

Widén, J., M. Lundh, I. Vassileva, E. Dahlquist, K. Ellegå rd, and E. Wäckelgå rd (2009,

July). Constructing load profiles for household electricity and hot water from time-use dataModelling approach and validation. *Energy and Buildings 41*(7), 753–768.

Woyte, A., V. V. Thong, R. Belmans, and J. Nijs (2006). Voltage fluctuations on distribution level introduced by photovoltaic systems. *IEEE Transactions on Energy Conversion 21*(1), 202–209.

Zurigat, Y. H., K. J. Maloney, and A. J. Ghajar (1989). A comparison study of one-dimensional models for stratified thermal storage tanks. *Journal of Solar Energy Engineering;(USA) 111*(3).